


Key Magnetized Exosomes for Effective Targeted Delivery of Doxorubicin Against Breast Cancer Cell Types in Mice Model

Wei Xu^{1,2}, Keren Wang², Ke Wang³, Ye Zhao⁴, Zhaoying Yang², Xiuying Li¹ 

¹Scientific Research Center, China-Japan Union Hospital of Jilin University, Changchun, Jilin, People's Republic of China; ²Department of Breast Surgery, China-Japan Union Hospital of Jilin University, Changchun, Jilin, People's Republic of China; ³Gynecology and Obstetrics Department, China-Japan Union Hospital of Jilin University, Changchun, Jilin, People's Republic of China; ⁴Dermatological Department, China-Japan Union Hospital of Jilin University, Changchun, Jilin, People's Republic of China

Correspondence: Xiuying Li; Zhaoying Yang, Email lixuying@jlu.edu.cn; zyyang@jlu.edu.cn

Introduction: Exosomes (Exos) are promising drug delivery systems due to their low immunogenicity, minimal toxicity, high biocompatibility, and effective delivery capabilities. However, addressing the cardiotoxicity and other toxic side effects associated with anthracyclines has proven challenging.

Methods: In this study, we loaded doxorubicin (Dox) into Exos derived from human placental mesenchymal stem cells (MSCs) and modified them with carboxylated Fe₃O₄ nanoparticles (NPs) to create an Exo-Dox-NP delivery system. Using an external magnetic force (MF), we regulated the distribution of Exos for targeted Dox delivery in breast cancer treatment. We characterized and determined the drug-loading efficiency of Exo-Dox-NPs, their uptake by tumor cells, and the modulation of drug release. The therapeutic efficacy of Exo-Dox-NPs was evaluated through both in vitro and in vivo anti-tumor experiments.

Results: Our results indicated that Exo-Dox-NPs remain stable in the bloodstream while releasing the drug in the acidic environment of tumor cells and their lysosomes. As a drug delivery system, Exo-Dox-NPs enhanced Dox absorption by tumor cells, demonstrating high targeting specificity. Moreover, Exo-Dox-NPs inhibited the migration of breast cancer cells, as confirmed by scratch migration and Transwell Matrigel invasion assays. In vivo experiments confirmed the effective targeting and delivery of Dox to malignant tumors using Exo-Dox-NPs/MFs, with the Exo-Dox-NP/MF formulation exhibiting the most potent anti-tumor activity.

Conclusion: The utilization of Exos as carriers for Dox showed promising efficacy in breast cancer management. Carboxylated Fe₃O₄ NPs demonstrated to be suitable targeting agents, potentially advancing the development of natural nanocarriers for combination cancer therapy.

Keywords: breast cancer, doxorubicin, exosomes, carboxylated Fe₃O₄ nanoparticles, magnetic targeting

Introduction

Breast cancer rates in women have been gradually rising by approximately 0.5% annually since the mid-2000s, according to data from the American Cancer Society. In 2023, breast cancer accounted for 31% of newly diagnosed cancer cases in women.¹ Further, based on global data from 2022 published by the International Agency for Research on Cancer, breast cancer is identified as a prevalent neoplasm, following closely behind lung cancer.² Treatment for breast cancer typically involves a combination of approaches, including surgery, chemotherapy, radiation therapy, endocrine therapy, and immunotherapy. These methods have significantly improved the quality of life of patients with breast cancer and reduced mortality rates. Anthracycline drugs are the first-line chemotherapeutic agents for breast cancer and have a positive impact on the survival and prognosis of patients with breast cancer. However, their side effects, such as cardiotoxicity and bone marrow suppression, have limited the clinical application of anthracycline drugs.

Nanoparticle (NP)-based drug delivery systems (DDSs), such as liposomes, micelles, solid lipid particles, nanocapsules, and polymer NPs, are used to enhance the effectiveness of chemical and biological drugs. However, the clinical

translation of DDSs faces challenges including cytotoxicity and rapid clearance by the reticuloendothelial system (RES) and mononuclear phagocyte system (MPS).³ Doxorubicin (Dox)-loaded PEGylated liposomes are reported to extend the half-life of the drugs; however, they also induce immune reactions *in vivo* and accumulate in the liver, thereby reducing drug distribution in diseased tissues.^{4,5} In contrast, endogenous exosomes (Exos) show promise as efficient drug carriers due to their biocompatibility, high stability, long half-life, low immunogenicity and toxicity in normal tissues, high permeability across biological barriers, and tissue-targeting capabilities.⁶

Nearly all types of normal cells can produce Exos; thus, they are found in cell culture supernatants, plasma, serum, urine, saliva, milk, and other biological fluids. Exos carry biomolecules specifically derived from their parent cells; therefore, Exos derived from diverse cellular sources differ in terms of production rate, content, functionality, load, and other factors. Consequently, these differing characteristics potentially yield distinct therapeutic effects.⁷ Mesenchymal stem cells (MSCs) are multipotent stem cells that can be expanded and differentiated *in vitro*, and they secrete a substantial amount of Exos.⁷ MSCs adapt to the tumor microenvironment and also participate in tissue injury and repair processes, exhibiting therapeutic effects against cardiovascular diseases, neurological disorders, and spinal cord injuries.^{8–11} Exos derived from MSCs can also exert anti-tumor effects. For example, Exos derived from murine bone marrow MSCs suppress angiogenesis in breast cancer (4T1) by downregulating the expression of vascular endothelial growth factor.¹²

Precision medicine emphasizes targeted drug delivery to improve drug distribution, reduce drug dosage, and minimize side effects. Magnetic drug targeting (MDT) is a promising technique that uses an external magnetic field in combination with DDSs to guide drugs to the target site, thereby maximizing therapeutic efficacy. Magnetically responsive particles are required as DDSs for MDT. They should be small but robustly responsive to magnetic fields, highly biocompatible, possess low toxicity, good dispersibility, and can easily conjugate with various ligands.¹³ Among various superparamagnetic iron oxide nanoparticles (SPIONs), Fe₃O₄ NPs are the most extensively used in various biomedical applications. Specifically, they have been used as magnetic resonance imaging contrast agents and targeted drug carriers in clinical diagnosis and treatment.^{14,15}

Modifying NP surfaces with different functional groups gives them unique characteristics, making them suitable for various biomedical and industrial applications. The utilization of Exos in site-specific drug delivery requires surface modification of Exos with targeting ligands to achieve precise localization at the intended site of action. Surface modification of Exos can be accomplished through diverse approaches, such as genetic engineering, covalent conjugation, and non-covalent interactions, thereby enabling organ-specific targeting.¹⁶ Adding hydrophilic groups, such as sulfhydryl, carboxyl, or amino groups, prevents NPs from being rapidly engulfed by RESs or MPSs, thus improving their treatment outcomes.¹⁷ In this study, we developed an Exo-Dox-NP delivery system by encapsulating Dox in Exos and modifying it with carboxylated Fe₃O₄ NPs. This system specifically targets tumor tissues with the help of an external magnetic field. The exosomal barrier protects Dox from degradation, thereby boosting its delivery.

Materials and Methods

Cell Culture

MSCs were isolated from the placental tissues of parturients by our research group with approval from the Ethics Committee of the China-Japan Union Hospital, Jilin University, Changchun, China after informed written consent was obtained from the participants. Our study complies with the Helsinki Declaration. MSCs were cultured in Alpha-Minimum Essential Medium (α -MEM, Hyclone, Logan, UT, USA) supplemented with 10% fetal bovine serum (FBS, Gibco, Grand Island, CA, USA) and 1% penicillin-streptomycin (Sigma-Aldrich, St. Louis, MO, USA). MDA-MB-231 human breast cancer cells and 4T1 mouse breast cancer cells were procured from the American Type Culture Collection (ATCC) and cultured in High-glucose Dulbecco's modified Eagle's medium (DMEM, Hyclone) supplemented with 10% FBS and 1% penicillin-streptomycin. All cell lines were maintained at 37°C in a humidified atmosphere of 5% CO₂ in a cell culture incubator (SANYO, Osaka, Japan).

The Animal Studies Using a Mouse Model

This study was approved by the Animal Ethics and Welfare Committee of Jilin University and was conducted in accordance with the Guidelines for Ethical Review of Animal Welfare as well as the Guidelines for the Management and Use of Laboratory Animals. Female, nonobese diabetic/severe combined immunodeficiency (NOD SCID) mice (3–5 weeks old) were purchased from Beijing Huafukang Biotechnology Co., Ltd. (Beijing, China). To establish an orthotopic breast cancer model, the MDA-MB-231 cell suspension (5×10^6 cells) was injected into the right third mammary fat pad of NOD SCID mice.

Extraction and Concentration Measurement of Exos

When the fusion degree of MSCs reached 70–80%, they were washed twice with 5 mL of phosphate-buffered saline (PBS, Gibco) and then incubated in serum-free α -MEM for 48 h. Afterward, the supernatant of the MSC culture medium was collected and centrifuged at $200 \times g$ for 10 min at 4°C to remove dead cells (Thermo Fisher Scientific, Waltham, MA, USA), followed by centrifugation at $2000 \times g$ for 10 min to remove cell debris and apoptotic bodies. The resulting supernatant was further centrifuged at $10,000 \times g$ for 1 h to remove microvesicles. The resulting liquid was then concentrated using a 100-kDa membrane ultrafiltration discs (Millipore, Bedford, MA, USA) during centrifugation to obtain a solution containing Exos, and the upper layer was collected. This concentrated solution was mixed with an Exo extraction reagent (ExoQuick-TC, System Biosciences, San Jose, CA, USA) at a volume ratio of 5:1 and incubated overnight at 4°C . Finally, the mixture was centrifuged at $1500 \times g$ for 30 min at 4°C , and the resulting pellet was considered the extracted Exos. The Exos were resuspended in an appropriate amount of PBS and stored at -80°C for future use. The concentration of Exos was measured using a Micro BCA protein assay kit (Thermo Fisher Scientific).

Preparation of Exo-Dox-NPs

The Exo-Dox mixture was prepared using an ultrasonic loading method (Sonics Materials Inc., Newton, CT, USA). Exos and Dox (Sigma-Aldrich) were mixed at a 1:1 ratio. Ultrasonic treatment was performed at 20% amplitude with a 30-s on/off cycle. After each cycle, the mixture was allowed to cool for 2 min. This process was repeated for a total of six cycles. All the procedures were performed on ice. The loaded Exo-Dox solution was then incubated at 37°C for 1 h to allow complete membrane recovery of the Exos. Carboxylated Fe_3O_4 NPs (XF NANO, Nanjing, China) were added separately to the Exos and Exo-Dox solutions at a ratio of 1:5. The mixture was gently shaken at 200 rpm for 90 min at 4°C . Finally, ExoQuick-TC reagent was added to the solution at a ratio of 5:1. The mixture was then vertically positioned and incubated overnight at 4°C . Subsequently, centrifugation (Eppendorf, Germany) was performed at $1500 \times g$ for 30 min at 4°C .

Characterization of Fe_3O_4 NPs, Exos, Exo-NPs and Exo-Dox-NPs

Observation of General Morphology

Fe_3O_4 NPs, purified Exos, Exo-NPs, and Exo-Dox-NPs were resuspended in appropriate volumes of PBS. Cells were fixed with 1% glutaraldehyde at room temperature for 30 min. Subsequently, 10 μL of the mixture was dropped onto a copper grid pre-treated with ultraviolet light. After drying for 30 min, samples were stained twice with 1% uranyl acetate. The samples were imaged using Transmission electron microscopy (TEM, H7650, Hitachi, Tokyo, Japan) at 120 kV.

Particle Size Analysis

Purified Exos, Exo-NPs, and Exo-Dox-NPs were resuspended in PBS and diluted to the appropriate concentrations. Nanoparticle tracking analysis (NTA, Malvern Panalytical, Malvern, UK) was used to track the Brownian motion of the particle and analyze the average size and size distribution data at room temperature.

Detection of Exosomal Biomarkers

Surface-specific markers of Exos were analyzed using Western blotting (WB). MSCs were cultured to a stable state, and the collected cells were lysed with protein lysis buffer, protease inhibitors, and phosphatase inhibitors at a ratio of 100:1:1. Protein lysates and Exos were quantified using a bicinchoninic acid (BCA) protein concentration assay. After boiling at 100°C for 5 min, the lysates and Exos were subjected to sodium dodecyl sulfate-polyacrylamide gel

electrophoresis (SDS-PAGE). The proteins were then transferred onto polyvinylidene fluoride (PVDF, Millipore) membranes using a semi-dry transfer method. PVDF membranes containing cells and Exos were separately incubated with an anti-calnexin antibody (Proteintech, Chicago, IL, USA). The exosomal PVDF membrane was incubated with anti-TSG101, anti-CD9, and anti-CD63, all obtained from Proteintech. After incubation overnight at 4°C, the membranes were washed thrice and incubated with corresponding secondary antibodies (Proteintech) under light-protected conditions. Finally, the membranes were scanned and analyzed using a dual-color infrared laser imaging system (ODYSSEY, San Jose, CA, USA).

Measurement of the Encapsulation Efficiency (EE)

We prepared a series of Dox solutions with concentrations of 0.01, 0.02, 0.03, 0.04, 0.05, and 0.06 mg/mL by serial dilution. A UV spectrophotometer (BioTek, Winooski, VT, USA) was calibrated using PBS, and the absorbance peaks of known concentrations of Dox standard solutions at 254 nm were measured to construct a standard curve. The supernatant obtained after centrifugation during the preparation of the Exo-Dox-NPs was collected and appropriately diluted, and the absorbance at 254 nm was measured. The Dox content not encapsulated by the Exos was determined based on the standard curve. The EE of Dox was calculated using the following equation:

$$\text{EE (\%)} = (\text{Total amount of Dox added} - \text{Dox content in the supernatant}) / (\text{Total amount of Dox added}) \times 100.$$

In vitro Dox Release Assessment

One mL solution of Exo-Dox-NPs was placed in a cellulose dialysis bag with a molecular weight cutoff of 10 kDa. The dialysis bag was submerged in 10 mL of PBS release media with pH 7.4 and pH 5.0, respectively. The system was incubated in a light-protected orbital shaker (Servicebio, Wuhan, China) at 37°C and 100 rpm for 48 h. At intervals of 2, 4, 6, 8, 10, 12, 24, 30, 36, and 48 h, 1 mL of the PBS release medium was withdrawn, and its absorbance at 254 nm was measured using a UV spectrophotometer. Subsequently, 1 mL of fresh PBS at the corresponding pH was added to maintain the volume. The Dox content in the release medium was calculated based on a standard curve, and the release rate was evaluated.

In vitro Cellular Uptake Studies

Colocalization Analysis Using Confocal Fluorescence Microscopy

DiO (Bestbio, Shanghai, China) was added to the Exo-Dox-NPs and Exo-NPs solutions, followed by a 20-min incubation at 37°C. Excess DiO was removed by adding an excess amount of PBS, and the samples were extracted using ExoQuick-TC reagent and resuspended in a small amount of culture medium. In confocal culture dishes containing MDA-MB-231 cells, Hoechst (Bestbio) was added and gently mixed to stain the cell nuclei. DiO-labeled Exo-Dox-NPs, Exo-NPs, and Dox were then added to the confocal culture dish and incubated at 37°C for 1 h. Following fixation with 4% paraformaldehyde, the localization of Exo and Dox in the cells was visualized using confocal fluorescence microscopy (FV1000, Olympus, Tokyo, Japan). All procedures were performed in the dark.

Utilizing Flow Cytometry to Quantify and Analyze the Cellular Uptake

Exo-Dox-NPs, Dox, Exo-NPs, and blank culture medium were added to a six-well plate containing MDA-MB-231 cells. The plate was incubated at 37°C for 1 h. The samples were then washed twice with PBS, and the cells were harvested using trypsin (Sigma-Aldrich) digestion. The harvested cells were centrifuged at 1000 rpm for 5 min and washed once with PBS. Then, the cells were resuspended in 500 µL of PBS, and the uptake of the Dox signal in each group was measured using a flow cytometer (Beckman Coulter, Brea, CA, USA).

Cell Viability Assay

To assess the effect of Exo-Dox-NPs on the viability of MDA-MB-231 and 4T1 cells, we employed the cell counting kit-8 (CCK-8) assay (Beyotime Biotech Corporation, Shanghai, China). The CCK-8 assay comprises WST-8, a substrate that can undergo enzymatic reduction by intracellular dehydrogenases, resulting in the formation of a soluble yellow formazan dye. The quantity of formazan produced is directly proportional to the number of viable cells. Consequently,

this property enables direct assessment of cell proliferation and cytotoxicity by measuring the optical density (OD value) of the yellow soluble product, thereby serving as an indicator of changes in cell population. MDA-MB-231 and 4T1 cells were seeded in a 96-well plate at a density of 8×10^3 cells per well and incubated at 37°C with 5% CO₂ for 24 h. Following this, the cells were treated with Exo-NPs, Dox, and Exo-Dox-NPs for 24 h, with equivalent Dox concentrations ranging from 0, 0.25, 0.5, 1, 5, 10, 20, and 50 µg/mL. After being washed twice with PBS, each well received 100 µL of culture medium and 10 µL of CCK-8 reagent, which was followed by a 2-h incubation in a CO₂ incubator. The absorbance was measured at 450 nm using a microplate reader (TECAN, Grärfelfing, Switzerland), and cell viability was calculated using the following formula:

$$\text{Cell viability (\%)} = \frac{(\text{Experimental group OD value} - \text{Blank group OD value})}{(\text{Control group OD value} - \text{Blank group OD value})} \times 100.$$

In vitro Migration and Invasion Assays

MDA-MB-231 and 4T1 cells were seeded in a 24-well plate at a density of 1.5×10^5 cells per well, which included culture-inserts (Ibidi, Martinsried, Germany). After 24 h of cell attachment, the Ibidi culture-inserts were gently removed, creating distinct cell-free gaps. The wells were then washed twice with PBS, and serum-free culture medium was added to each well. The experimental groups were Exo-Dox NPs, Dox, and Exo-NPs. Images of the scratched areas were captured at 0, 6, 12, and 24 h using an inverted phase contrast microscope (Olympus).

For the Transwell assay, MDA-MB-231 and 4T1 cells were divided into four groups: control, Exo-NPs, Dox, and Exo-Dox-NPs. Matrigel (Corning, Corning, NY, USA) was diluted at 1:8 and 40 µL was added to the upper chamber of the Transwell insert (Corning). The plate was then incubated at 37°C for 4 h to allow Matrigel to gel. MDA-MB-231 cells were digested, centrifuged, washed twice with PBS, and resuspended in a serum-free culture medium. The cell density was adjusted to 8×10^5 cells per mL. A volume of 100 µL of cell suspension was added to the Transwell chamber with an 8-µm pore size, while 500 µL of culture medium containing 20% FBS was added to the lower chamber of the 24-well plate. The plates were incubated for 24 h. Subsequently, the Transwell insert was removed, and the chamber was washed twice with PBS. The Matrigel and cells in the upper chamber were removed using a cotton swab. Cells in the 24-well plates were fixed with 4% paraformaldehyde for 30 min. Staining was performed by applying 0.1% crystal violet and leaving it 15 min, followed by three washes with PBS. Cells were counted in five fields at 400× magnification under an inverted phase contrast microscope.

In vivo Targeting and Biodistribution

We established a transplant tumor model of MDA-MB-231 in NOD SCID mice. The mice were randomly assigned to one of the following five groups: PBS, Exo-NPs, Dox, Exo-Dox-NPs, and Exo-Dox-NPs/MF. Mice in the PBS group received intravenous (i.v.) injections of PBS, while those in the Exo-NPs group received i.v. injections of Exo-NPs. Similarly, mice in the Dox group received i.v. injections of Dox, and those in the Exo-Dox-NP group received i.v. injections of Exo-Dox-NP. The Exo-Dox-NPs/MF group received the same treatment as the Exo-Dox-NP group, along with the placement of a 1.2T magnet at the tumor site for 30 min. At 6, 12, and 24 h after administration, the mice were euthanized, and the heart, liver, kidney, lung, spleen, and tumor were collected and washed with saline. Fluorescence enrichment images of the mice were acquired using a small-animal imaging system (IVIS, KODAK, Rochester, NY, USA).

In vivo Anti-Tumor Effects

When the tumor volume of the mice reached 100 mm³ (tumor volume = length × width²/2), they were randomly assigned to one of the five groups: PBS, Exo-NPs, Dox, Exo-Dox-NPs, and Exo-Dox-NPs/MF, with five mice in each group. The mice received intravenous injections of the drugs every three days, with a dose equivalent to 3 mg/kg of Dox. In the Exo-Dox-NPs/MF group, a 1.2T magnet was placed at the tumor site for 30 min. According to the Guidelines for Ethical Review of Animal Welfare, during the 16-day treatment period, the body weights and tumor volumes should be monitored, and the tumor diameter should not exceed 1.5 cm. After 16 days of treatment, the mice were euthanized, and their hearts and tumor specimens were harvested and tumor weights recorded.

Histology and Immunohistochemistry

After euthanizing the mice, tumor tissues and internal organs were dissected and then fixed in 4% paraformaldehyde for 24 h. The hearts were embedded in paraffin, and tissue sections were stained with hematoxylin and eosin (H&E) stain to observe drug-induced cardiac toxicity. The tumor tissue was subjected to immunohistochemical analysis using the Ki-67 antibody to observe the proliferation of tumor cells. Cell apoptosis in tumor tissues was evaluated using the terminal deoxynucleotidyl transferase dUTP nick end labeling (TUNEL) fluorescence assay.

Statistical Analyses

All data were obtained from a minimum of three independent experiments and are presented as the mean \pm standard deviation (SD). Data were analyzed using GraphPad Prism 10.1.2 software, and the statistical significance of differences between groups was assessed using a one-way analysis of variance or a *t*-test. Statistical significance was set at $p < 0.05$.

Results

Morphological and Structural Characterization of Various Nanoparticles

TEM was used to examine the shapes and structures of Fe₃O₄ NPs, Exos, Exo-NPs, and Exo-Dox-NPs using an accelerated electron beam. The TEM images revealed that Fe₃O₄ NPs were uniformly spherical with diameters of about 5–10 nm (Figure 1A). Exos appeared as circular or elliptical cup-shaped vesicles, ranging from 30 to 200 nm in diameter, and exhibited a lipid bilayer membrane, which is typical for Exos. Electron microscopy analysis of Exo-NPs

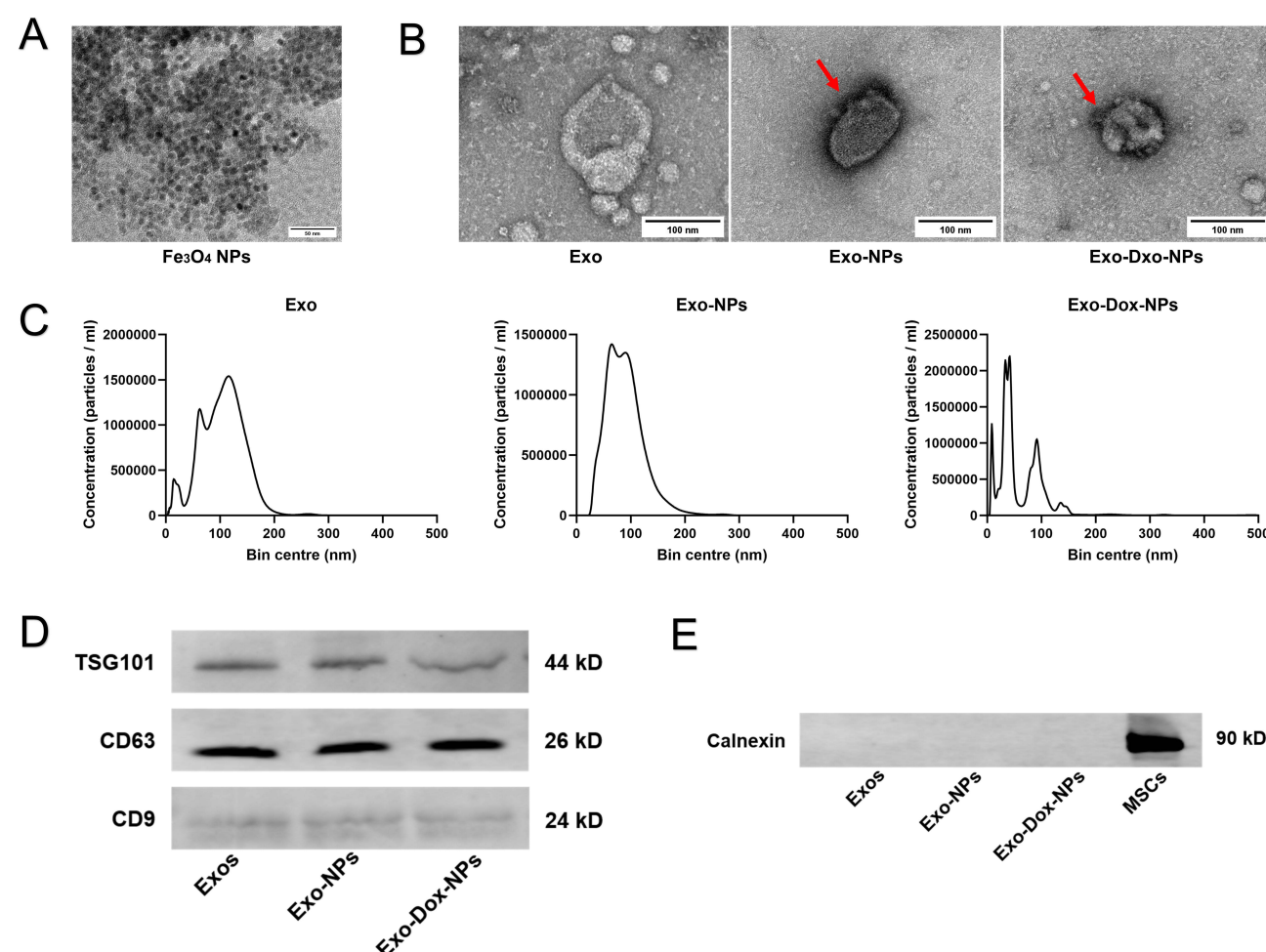


Figure 1 Characterization of the nanoparticles. (A) TEM images of Fe₃O₄ NPs. Scale bar, 50 nm. (B) Representative TEM images of Exos, Exo-NPs, and Exo-Dox-NPs (The arrows indicate Fe₃O₄ NPs attached to the surface of Exos). Scale bar, 100 nm. (C) Size distribution of Exos, Exo-NPs, and Exo-Dox-NPs. (D) Western blot analysis of the Exo-, Exo-NP-, and Exo-Dox-NP- marker proteins TSG101, CD63, and CD9. (E) Analysis of Calnexin in the endoplasmic reticulum of MSCs, Exos, Exo-NPs, and Exo-Dox-NPs.

and Exo-Dox-NPs demonstrated that Fe_3O_4 NPs were attached to the biomembranes (Figure 1B). These observations suggested that the circular and vesicular shapes of Exos remained stable during drug encapsulation.

NTA was used to quantify size distributions using particle light scattering and Brownian motion. Our NTA result demonstrated that Exos diameter was largely concentrated in the range of 30–200 nm, with an average particle size of 104.8 ± 1.8 nm and a peak size of 96.6 ± 9.1 nm. Exo-NPs had an average particle size of 90.0 ± 3.2 nm, with a peak size of 87.8 ± 7.1 nm. In contrast, Exo-Dox-NPs had a smaller average size of 55.3 ± 8.6 nm, with a peak size of 25.0 ± 6.9 nm (Figure 1C). The observed changes in diameter were potentially influenced by the properties of the drug and loading method used.

Western blot analysis was performed to detect surface markers of Exos. We found the expression of Exos-specific markers, including tetraspanins (CD9 and CD63) and the multivesicular body (MVB) formation-associated protein (TSG101) (Figure 1D). Specific Exos markers were also present in Exo-NPs and Exo-Dox-NPs, indicating that drug loading did not significantly affect the presence of these protein markers. Since Exos, a subpopulation of extracellular vesicles, are derived from cells, they typically lack the endoplasmic reticulum protein Calnexin (Figure 1E). This result was also true in our experiments, confirming the purity of our Exos and their freedom from cellular impurities.

Loading and Release Kinetics of Doxorubicin from Exosome-Encapsulated Nanoparticles

Exosomes were loaded with Dox at a ratio of 1:1 using an ultrasound-assisted method. The loaded Exos were then co-incubated with Fe_3O_4 NPs at a ratio of 5:1. Standard solutions of Dox were prepared at various different concentrations, and the absorbance peaks at approximately 254 nm were measured using a UV spectrophotometer (Figure 2A). The Dox concentration in the test samples was determined using the standard curve, and the EE was found to be approximately 38% based on volumetric quantification (Figure 2B).

Exo-Dox-NPs exhibited significantly higher drug release rates and amounts in the intracellular environment compared to the physiological environment simulated by PBS at pH 7.4 and pH 5.0, respectively. Drug release from Exo-Dox-NPs showed an initial burst within the first 6 h, followed by a sustained release phase. Under acidic conditions, Exo-Dox-NPs released about 80% of the drug after 48 h, indicating a notable degree of sustained release capability (Figure 2C). Thus, NPs used in our study appear to remain stable in the bloodstream but can be triggered to release drugs in the acidic environment of tumor cells and lysosomes.

Cellular Uptake of Exo-Dox-NPs in Tumor Cells

Purified Exos can be tagged with fluorescent dyes to study their cellular targeting, uptake, internalization pathways, cellular transport, in vivo biodistribution, and tissue accumulation using confocal fluorescence microscopy. The fluorescent lipophilic dye DiO binds to the lipid bilayer of exosomal membranes, whereas the Hoechst live cell staining solution stains the cell nucleus. Our confocal fluorescence microscopy analysis demonstrated the uptake of Exo-Dox-NPs by tumor cells (Figure 2D).

Exos can be internalized by cells through various mechanisms, such as membrane fusion, endocytosis, and receptor interactions, enabling them to transport and release bioactive substances within recipient cells. After a 1-h incubation with cells in a six-well plate, we analyzed cellular uptake levels using flow cytometry. This analysis of MDA-MB-231 cells demonstrated that the binding of Exo-Dox-NPs to tumor cells was more effective than that of free Dox (96.06% vs 60.53%) (Figure 2E). These experiments clearly indicate that, as a drug delivery system, Exo-Dox-NPs facilitate Dox uptake by tumor cells, exhibiting high targeting specificity.

In vitro Assessment of Anti-Tumor Effects of Exo-Dox-NPs

Cell viability was assessed using the CCK-8 assay, where the OD values reflected changes in cell numbers and were used to evaluate how well Exo-Dox-NPs killed tumor cells. We noticed similar outcomes for both MDA-MB-231 and 4T1 cells, demonstrating that Exo-Dox-NPs had a strong inhibitory effect on cell proliferation (Figure 3A). The efficiency of cell growth inhibition by Exo-Dox-NPs was comparable to that of free Dox, confirming the high efficiency of Dox

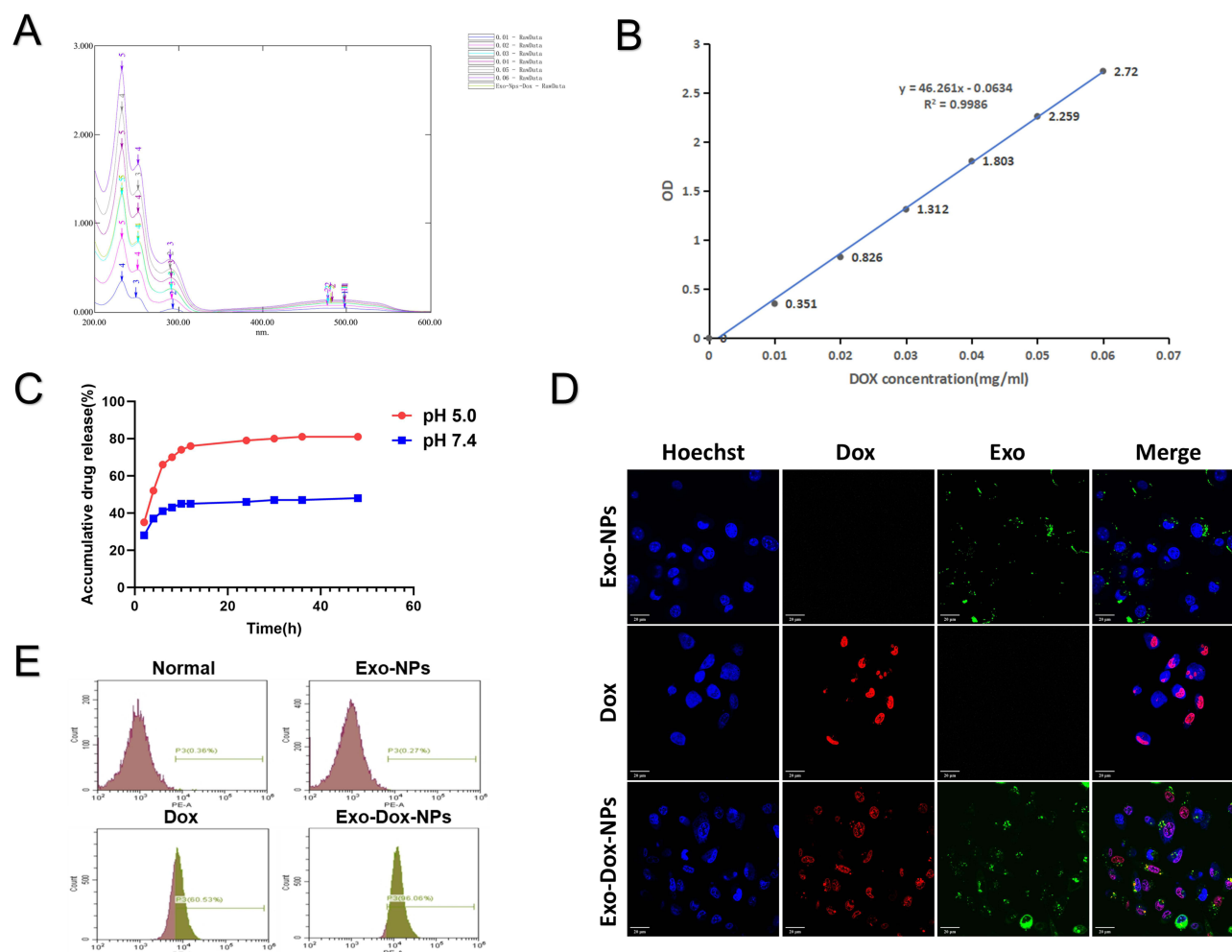


Figure 2 In vitro validation of the drug encapsulation efficiency, drug release efficacy, and cellular uptake of Exo-Dox-NPs. (A) UV-Vis spectrophotometric spectra of Dox at concentrations of 0.01, 0.02, 0.03, 0.04, 0.05, and 0.06 mg/mL. (B) Standard curve of Dox concentration. (C) In vitro release of Dox at pH 5.0 and 7.4. (D) Intracellular colocalization of Exos membranes (DiO, green) and Dox (red). MSC nuclei were stained with Hoechst (blue). Scale bar, 20 μ m. (E) Flow cytometry analysis of Dox uptake efficiency by breast cancer cells.

delivery via Exo-Dox-NPs. In contrast, no significant inhibition of cell growth was observed in the Exo-NP group, indicating that Exo-NPs exhibited low or no toxicity.

The scratch migration assay evaluated the influence of Exo-Dox-NPs on the migration of tumor cells. Both Exo-Dox-NPs and Dox affected the migration speed and rate of MDA-MB-231 and 4T1 cells, showing a significant reduction compared to those of the control group (Figure 3B). These findings indicate that Exo-Dox-NPs hinders the spread of breast cancer cells.

Furthermore, we conducted a Transwell invasion assay, where tumor cells were seeded in the upper chamber and FBS was placed in the lower chamber to provide a higher concentration of nutrients. To mimic the extracellular matrix in vivo, a layer of Matrigel was applied to the upper side of the Transwell membrane. In this setup, tumor cells need to secrete matrix metalloproteinases (MMPs) to degrade Matrigel and migrate through the Transwell membrane into the lower chamber. Quantifying of the cells that migrated into the lower chamber allowed us assess the invasive capacity of the tumor cells. Exo-Dox-NPs significantly reduced the invasion of breast cancer cells, as evidenced by the results of the Transwell Matrigel invasion assay (Figure 3C and D).

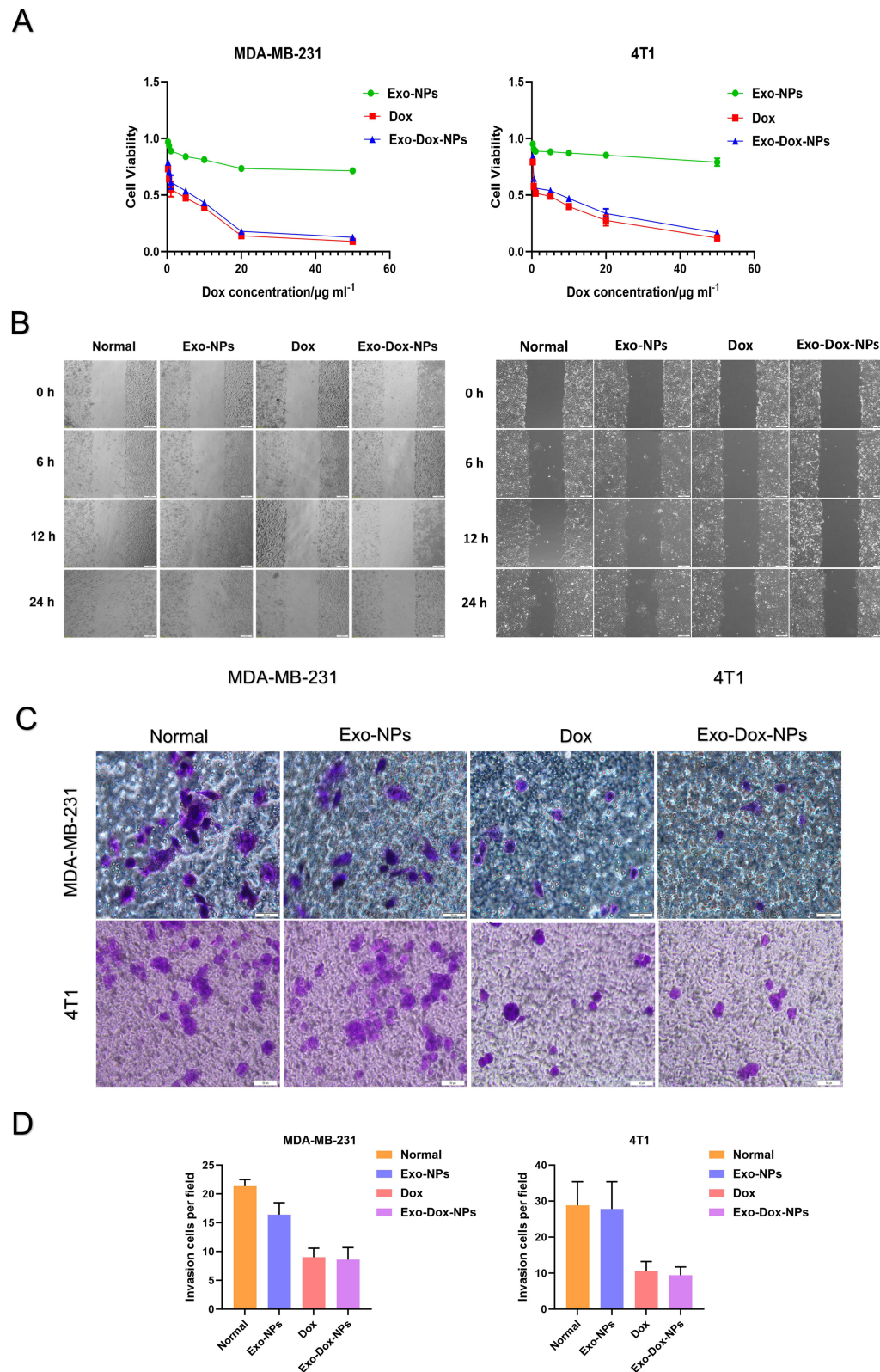


Figure 3 In vitro inhibitory effect of Exo-Dox-NPs on breast cancer cells. **(A)** CCK-8 assay to evaluate the cytotoxic effects of Dox and Exo-Dox-NPs at different concentrations on breast cancer cells. **(B)** Effect of Exo-Dox-NPs on the migration ability of breast cancer cells. Scale bar, 100 μm . **(C)** Effect of Exo-Dox-NPs on the invasion ability of breast cancer cells. Scale bar, 50 μm . **(D)** Number of cells that penetrated Matrigel and migrated to the lower chamber of the Transwell.

In vivo Targeting and Biodistribution of Exo-Dox-NPs in Tumor Tissues

To evaluate how well Exo-Dox-NPs target tumors *in vivo*, we injected mice with these NPs via the tail vein. Fluorescence imaging was conducted at 6, 12, and 24 h post-administration to track their distribution in the mice. No specific fluorescence was detected in the organs or tumor tissues of mice in the PBS and Exo-NP groups. However, in the Exo-Dox-NPs/MF group, substantial fluorescence accumulation was observed in the tumor region between 6 and 12 h post-administration. In contrast, the free Dox and Exo-Dox-NP groups exhibited higher accumulation in the liver by the 24-h mark. The fluorescence intensity in the Dox and Exo-Dox-NP groups appeared weaker than that in the Exo-Dox-NPs/MF group, suggesting the effective active targeting effect of Exo-Dox-NPs/MF. Overall, Exo-Dox-NPs/MFs exhibited excellent performance in targeting and delivering Dox to malignant tumors (Figure 4A).

In vivo Efficacy of Exo-Dox-NPs in Tumor Tissues

We analyzed the effectiveness of tumor treatment in each group. The average tumor volumes in the Exo-Dox-NP and Exo-Dox-NP/MF groups were significantly smaller than those in the PBS, Exo-NP, and Dox groups (Figure 4B and C). Except for the free Dox group, there were no significant differences in the average body weight among the other treatment groups, indicating a lower systemic toxicity of our treatment regimen (Figure 4D). In addition, the average tumor weight was significantly lower in the Exo-Dox-NP and Exo-Dox-NPs/MF groups than in the PBS and Exo-NP groups. Furthermore, there was a statistically significant difference in tumor weight between the Exo-Dox-NPs/MF and Exo-Dox-NP groups (Figure 4E). These results confirmed the synergistic effect of Exos and Dox on malignant breast tumors in living organisms, emphasizing the effectiveness of magnetic targeting.

Cardiotoxicity and Tumor Dynamics Analysis Following Exo-Dox-NPs Treatment

We employed H&E staining on mouse heart tissues to compare the cardiotoxicity of Exo-Dox-NPs with that of free Dox. No significant damage to myocardial tissues was observed in the Exo-NP group compared with the PBS group. In contrast, the free Dox group exhibited clear signs of myocardial damage, including cell swelling, degeneration, necrosis, cytoplasmic vacuolar degeneration, and myocardial fiber rupture. The use of Exo-loaded Dox significantly reduced cardiotoxicity, suggesting that the DDS we developed is biocompatible and safer than Dox alone.

Immunohistochemical staining with anti-Ki-67 antibody was performed on mouse tumor samples to investigate tumor cell proliferation. The positive rates of Ki-67 in the tumor tissues of the Exo-Dox-NPs, Dox and Exo-Dox-NPs/MF groups were lower than those in the PBS group, indicating that Exos had a significant inhibitory effect on tumor cell proliferation.

We also performed a TUNEL fluorescence staining analysis of mouse tumor tissues to detect cell apoptosis. The effectiveness of the treatment was evaluated by quantifying the number and distribution of apoptotic cells in the tumor tissues. The Exo-Dox-NPs/MF group exhibited the highest levels of green fluorescence, indicating the greatest extent of tumor cell apoptosis. This observation suggests that the Exo-Dox-NP/MF formulation possesses the strongest anti-tumor activity (Figure 4F).

Discussion

In this study, we selected MDA-MB-231 and 4T1 cells as research models, both of which represent triple-negative breast cancer (TNBC) cell lines. Compared to other subtypes breast cancer, TNBC patients exhibit the lowest rates of metastasis-free survival and overall survival.¹⁸ The main therapeutic approach for patients with TNBC involves conventional systemic chemotherapy with cytotoxic agents. However, using Dox as a frontline chemotherapeutic agent can increase susceptibility to cardiovascular disorders. To address this, we have engineered the Exo-Dox-NPs drug delivery platform.

Although various methods exist for isolating and purifying Exos, each has its limitations. In our study, we combined ultracentrifugation, ultrafiltration, and reagent extraction methods to isolate and purify Exos, aiming for improved yield and purity. Further research is needed to determine the optimal Exos-to-drug ratio, which can significantly affect loading efficiency. Some studies have used exosome/drug ratios of 9:1 and 4:1 for lipophilic drugs,^{19,20} while research on

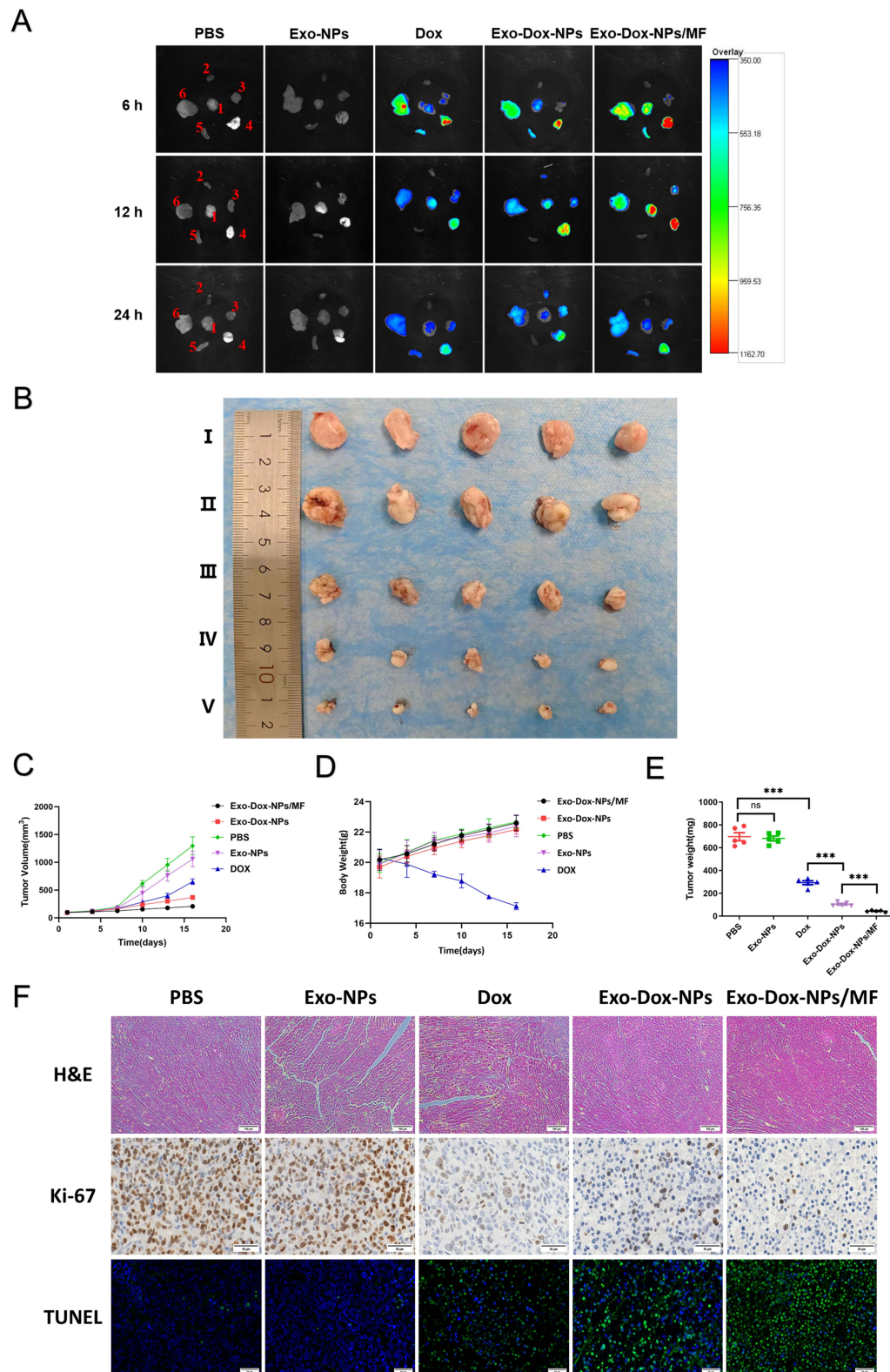


Figure 4 In vivo anti-tumor effects of Exo-Dox-NPs. **(A)** In vitro fluorescence imaging of tumor-bearing NOD SCID mice at 6, 12, and 24 h post-injection of the nanoparticles (I, tumor; 2, Heart; 3, kidney; 4, lung; 5, spleen; 6, liver). **(B)** Tumor-bearing mice were administered the drug (3 mg/kg Dox) via tail vein injection every 3 days for 16 days. After treatment completion, macroscopic photographs of the excised tumors were taken (I, PBS; II, Exo-NPs; III, Dox; IV, Exo-Dox-NPs; V, Exo-Dox-NPs/MF). **(C)** Tumor growth during treatment, **(D)** body weight changes during treatment and **(E)** tumor weight after treatment ($n = 5$; data is presented as mean \pm SD *** $p < 0.001$, ns non significant). **(F)** H&E staining of heart tissue (scale bar, 100 μ m), IHC analysis of Ki67 (scale bar, 50 μ m), and TUNEL staining of tumor tissue (scale bar, 50 μ m).

hydrophilic drugs typically employs 1:1 ratio.²¹ Therefore, we mixed Exos with Dox—a hydrophilic chemotherapeutic agent—in a 1:1 ratio to load the drug into the Exos.

To validate the purification of Exo as targeting nanocarriers, we characterized their shape, size, stability, and membrane protein markers. In studies related to drug loading and surface modification of Exos, the particle diameter may either increase or decrease compared to that of blank Exos due to the loading or modification procedures.^{22,23} The difference in size may result from the presence of carboxyl-functionalized superparamagnetic Fe₃O₄ NPs on the surface of the Exos and the ultrasound-assisted drug-loading process. The introduction of surface charge and functional groups to Fe₃O₄ NPs may have altered the surface properties of the Exos, or surface tension of Exos, influencing attractive or repulsive interactions between Exos and the surrounding molecules in solution. Such change in surface properties may have affected the aggregation dispersion and particle size of Exos. Furthermore, Fe₃O₄ NPs may have formed a dense encapsulation layer on the surface of Exos, reducing their size. Additionally, the mechanical shear forces and microvortices generated during the ultrasound-assisted Dox loading process may have also disrupted the aggregation state of Exos, promoting their dispersion and reducing particle size.

We assessed the drug release under two conditions PBS at pH 7.4 and pH 5, mimicking physiological and intracellular environments, respectively. The formulation remained stable in the bloodstream, whereas the acidic environment of the intracellular and lysosomal compartments triggered drug release. It should be noted that a slightly acidic pH in the tumor microenvironment enhanced the uptake of Exos by tumor cells. This facilitation is likely due to the presence of ganglioside GM3 in the Exos membrane, which carries a positive charge in acidic conditions, resulting in better cellular uptake than at the physiological pH.²⁴

We evaluated the inhibitory effects of Exo-Dox-NPs on tumor cells in vitro using a standard cell viability assay. The results showed slightly higher cellular toxicity of free Dox compared to Exo-Dox-NPs, likely due to the smaller size and faster cellular penetration of free Dox.²⁵ The slow release of encapsulated Dox and the structural stability of Exos provide significant advantages as carriers. Our findings are aligned with those of Hosseini et al and Bagheri et al^{26,27} On the contrary, Schindler et al reported that extracellular vesicles encapsulating Dox exhibited approximately 20-fold higher in vitro cytotoxicity than free Dox.²⁸ In addition, our results indicated significantly enhanced suppression of migration and invasion in breast cancer cells upon treatment with Exo-Dox-NPs, surpassing the inhibitory effects exerted by free Dox. These findings suggest that Exos exhibit superior biocompatibility as drug carriers.

We also evaluated the in vivo anti-tumor efficacy of Exo-Dox-NPs and found that, under the influence of an external magnetic field, the Exo-Dox-NPs/MF group exhibited improved drug retention and therapeutic efficacy. A major advantage of nanoscale DDS in cancer therapy is the EPR effect, which facilitates selectively accumulation of nanoscale particles and vesicles in tumors owing to their enhanced permeability and prolonged retention in tumor vasculature leakage.²⁹ Through the EPR effect, Exos minimize non-specific binding to non-targeted sites while concentrating drugs at tumor sites. Moreover, we used an external magnetic field to actively target and transport Exos to the tumor site by guiding Fe₃O₄ NPs, resulting in improved therapeutic outcomes.

Conclusion

In this study, we successfully constructed a Exo-Dox-NPs drug delivery system. We found that loading Dox into Exos and modifying their surface with Fe₃O₄ NPs did not affect the biological characteristics of Exos while effectively integrating them into tumor cells. Dox encapsulated in Exos significantly reduced cardiac toxicity and prolonged effectiveness. In the presence of an external magnetic field, Fe₃O₄ NPs exhibited active targeting towards the tumor site, thereby augmenting the selectivity of Exos-mediated drug delivery. Hence, our research substantiates the potential of the Exo-Dox-NPs drug delivery system in efficaciously addressing breast tumors. This methodology contributes to the advancement of innate nanocarriers and presents the possibility of intricate dosing regimens in the future through modulation of magnetic field intensity.

Data Sharing Statement

All data generated or analyzed during this study are included in the publication.

Acknowledgments

We are grateful to the following staffs for the guidance and support of flow cytometry: Yucheng Zhang, Liu Yingnan, and Lv Huiying.

Funding

The present study was supported by the National Natural Science Funds of China (No. 82000765), the Education Department of Jilin Province (No. JJKH20211148KJ), the Department of Science and Technology of Jilin Province (YDZJ202401195ZYTS, 20210203215SF, YDZJ202301ZYTS098), the Spring Bud Project of China-Japan Union Hospital of Jilin University (No. 2023CL03) and the Project of Technical Service (No. 2024YX0095).

Disclosure

The authors report no conflicts of interest in this work.

References

1. Siegel RL, Miller KD, Wagle NS, Jemal A. Cancer statistics, 2023. *CA Cancer J Clin*. 2023;73(1):17–48. doi:10.3322/caac.21763
2. Bray F, Laversanne M, Sung H, et al. Global cancer statistics 2022: GLOBOCAN estimates of incidence and mortality worldwide for 36 cancers in 185 countries. *CA Cancer J Clin*. 2024;74(3):229–263. doi:10.3322/caac.21834
3. Haque S, Whittaker MR, McIntosh MP, Pouton CW, Kaminskas LM. Disposition and safety of inhaled biodegradable nanomedicines: opportunities and challenges. *Nanomedicine*. 2016;12(6):1703–1724. doi:10.1016/j.nano.2016.03.002
4. Suk JS, Xu Q, Kim N, Hanes J, Ensign LM. PEGylation as a strategy for improving nanoparticle-based drug and gene delivery. *Adv Drug Deliv Rev*. 2016;99(Pt A):28–51. doi:10.1016/j.addr.2015.09.012
5. Chow TH, Lin YY, Hwang JJ, et al. Improvement of biodistribution and therapeutic index via increase of polyethylene glycol on drug-carrying liposomes in an HT-29/luc xenografted mouse model. *Anticancer Res*. 2009;29(6):2111–2120.
6. Li J, Zhang Y, Dong PY, Yang GM, Gurunathan S. A comprehensive review on the composition, biogenesis, purification, and multifunctional role of exosome as delivery vehicles for cancer therapy. *Biomed Pharmacother*. 2023;165:115087. doi:10.1016/j.biopha.2023.115087
7. Zhang Y, Bi J, Huang J, Tang Y, Du S, Li P. Exosome: a Review of Its Classification, Isolation Techniques, Storage, Diagnostic and Targeted Therapy Applications. *Int J Nanomed*. 2020;15:6917–6934. doi:10.2147/ijn.S264498
8. Yin S, Ji C, Wu P, Jin C, Qian H. Human umbilical cord mesenchymal stem cells and exosomes: bioactive ways of tissue injury repair. *Am J Transl Res*. 2019;11(3):1230–1240.
9. Arslan F, Lai RC, Smeets MB, et al. Mesenchymal stem cell-derived exosomes increase ATP levels, decrease oxidative stress and activate PI3K/Akt pathway to enhance myocardial viability and prevent adverse remodeling after myocardial ischemia/reperfusion injury. *Stem Cell Res*. 2013;10(3):301–312. doi:10.1016/j.scr.2013.01.002
10. Cui GH, Wu J, Mou FF, et al. Exosomes derived from hypoxia-preconditioned mesenchymal stromal cells ameliorate cognitive decline by rescuing synaptic dysfunction and regulating inflammatory responses in APP/PS1 mice. *FASEB j*. 2018;32(2):654–668. doi:10.1096/fj.201700600R
11. Li L, Zhang Y, Mu J, et al. Transplantation of Human Mesenchymal Stem-Cell-Derived Exosomes Immobilized in an Adhesive Hydrogel for Effective Treatment of Spinal Cord Injury. *Nano Lett*. 2020;20(6):4298–4305. doi:10.1021/acs.nanolett.0c00929
12. Lee JK, Park SR, Jung BK, et al. Exosomes derived from mesenchymal stem cells suppress angiogenesis by down-regulating VEGF expression in breast cancer cells. *PLoS One*. 2013;8(12):e84256. doi:10.1371/journal.pone.0084256
13. Wahajuddin AS. Superparamagnetic iron oxide nanoparticles: magnetic nanoplateforms as drug carriers. *Int J Nanomed*. 2012;7:3445–3471. doi:10.2147/ijn.S30320
14. Amstad E, Zurcher S, Mashaghi A, Wong JY, Textor M, Reimhult E. Surface functionalization of single superparamagnetic iron oxide nanoparticles for targeted magnetic resonance imaging. *Small*. 2009;5(11):1334–1342. doi:10.1002/sml.200801328
15. Ruoslahti E, Bhatia SN, Sailor MJ. Targeting of drugs and nanoparticles to tumors. *J Cell Biol*. 2010;188(6):759–768. doi:10.1083/jcb.200910104
16. Salunkhe S, Basak M, Chitkara D, Mittal A. Surface functionalization of exosomes for target-specific delivery and in vivo imaging & tracking: strategies and significance. *J Control Release*. 2020;326:599–614. doi:10.1016/j.jconrel.2020.07.042
17. Harris JM, Chess RB. Effect of pegylation on pharmaceuticals. *Nat Rev Drug Discov*. 2003;2(3):214–221. doi:10.1038/nrd1033
18. Li Y, Wang S, Yang W, Liu H. Prognostic significance of molecular subtype, metastatic site and primary tumor surgery for survival in primary metastatic breast cancer: a SEER-based study. *Medicine*. 2021;100(27):e26619. doi:10.1097/md.00000000000026619
19. Munagala R, Aqil F, Jeyabalan J, Gupta RC. Bovine milk-derived exosomes for drug delivery. *Cancer Lett*. 2016;371(1):48–61. doi:10.1016/j.canlet.2015.10.020
20. Kalani A, Chaturvedi P, Kamat PK, et al. Curcumin-loaded embryonic stem cell exosomes restored neurovascular unit following ischemia-reperfusion injury. *Int J Biochem Cell Biol*. 2016;79:360–369. doi:10.1016/j.biocel.2016.09.002
21. Gomari H, Forouzandeh Moghadam M, Soleimani M, Ghavami M, Khodashenas S. Targeted delivery of doxorubicin to HER2 positive tumor models. *Int J Nanomed*. 2019;14:5679–5690. doi:10.2147/ijn.S210731
22. Wei H, Chen F, Chen J, et al. Mesenchymal Stem Cell Derived Exosomes as Nanodrug Carrier of Doxorubicin for Targeted Osteosarcoma Therapy via SDF1-CXCR4 Axis. *Int J Nanomed*. 2022;17:3483–3495. doi:10.2147/ijn.S372851
23. Gong C, Tian J, Wang Z, et al. Functional exosome-mediated co-delivery of doxorubicin and hydrophobically modified microRNA 159 for triple-negative breast cancer therapy. *J Nanobiotechnol*. 2019;17(1):93. doi:10.1186/s12951-019-0526-7
24. Parolini I, Federici C, Raggi C, et al. Microenvironmental pH is a key factor for exosome traffic in tumor cells. *J Biol Chem*. 2009;284(49):34211–34222. doi:10.1074/jbc.M109.041152

25. Ye M, Han Y, Tang J, et al. A Tumor-Specific Cascade Amplification Drug Release Nanoparticle for Overcoming Multidrug Resistance in Cancers. *Adv Mater*. 2017;29(38). doi:10.1002/adma.201702342
26. Hosseini NF, Amini R, Ramezani M, Saidijam M, Hashemi SM, Najafi R. AS1411 aptamer-functionalized exosomes in the targeted delivery of doxorubicin in fighting colorectal cancer. *Biomed Pharmacother*. 2022;155:113690. doi:10.1016/j.biopha.2022.113690
27. Bagheri E, Abnous K, Farzad SA, Taghdisi SM, Ramezani M, Alibolandi M. Targeted doxorubicin-loaded mesenchymal stem cells-derived exosomes as a versatile platform for fighting against colorectal cancer. *Life Sci*. 2020;261:118369. doi:10.1016/j.lfs.2020.118369
28. Schindler C, Collinson A, Matthews C, et al. Exosomal delivery of doxorubicin enables rapid cell entry and enhanced in vitro potency. *PLoS One*. 2019;14(3):e0214545. doi:10.1371/journal.pone.0214545
29. Blanco E, Shen H, Ferrari M. Principles of nanoparticle design for overcoming biological barriers to drug delivery. *Nat Biotechnol*. 2015;33(9):941–951. doi:10.1038/nbt.3330

International Journal of Nanomedicine

Dovepress

Publish your work in this journal

The International Journal of Nanomedicine is an international, peer-reviewed journal focusing on the application of nanotechnology in diagnostics, therapeutics, and drug delivery systems throughout the biomedical field. This journal is indexed on PubMed Central, MedLine, CAS, SciSearch®, Current Contents®/Clinical Medicine, Journal Citation Reports/Science Edition, EMBase, Scopus and the Elsevier Bibliographic databases. The manuscript management system is completely online and includes a very quick and fair peer-review system, which is all easy to use. Visit <http://www.dovepress.com/testimonials.php> to read real quotes from published authors.

Submit your manuscript here: <https://www.dovepress.com/international-journal-of-nanomedicine-journal>